SUPPORTING INFORMATION

Layered $Zn_2[Co(CN)_6](CH_3COO)$ double metal cyanide: a two-dimensional DMC phase with excellent catalytic performance

Carlos Marquez,[a] Arkadiy Simonov,[b] Michael T. Wharmby,[c] Cédric Van Goethem,[a] Ivo Vankelecom,[a] Bart Bueken,[a] Andraž Krajnc,[d] Gregor Mali,[d] Dirk De Vos*[a] and Trees De Baerdemaeker*[a]

[a] Centre for Surface Chemistry and Catalysis, KU Leuven, Celestijnenlaan 200F p.o. box 2461, 3001 Leuven, Belgium.

[b] Inorganic Chemistry Laboratory, University of Oxford, South Parks Road, Oxford OX1 3QR, United Kingdom.

[c] Deutsches Elektronen-Synchrotron (DESY), Notkestraße 85, 22607 Hamburg, Germany.

[d] Department of Inorganic Chemistry and Technology, National Institute of Chemistry, Hajdrihova 19, 1001 Ljubljana, Slovenia.

*Corresponding authors: dirk.devos@kuleuven.be; trees.debaerdemaeker@kuleuven.be.

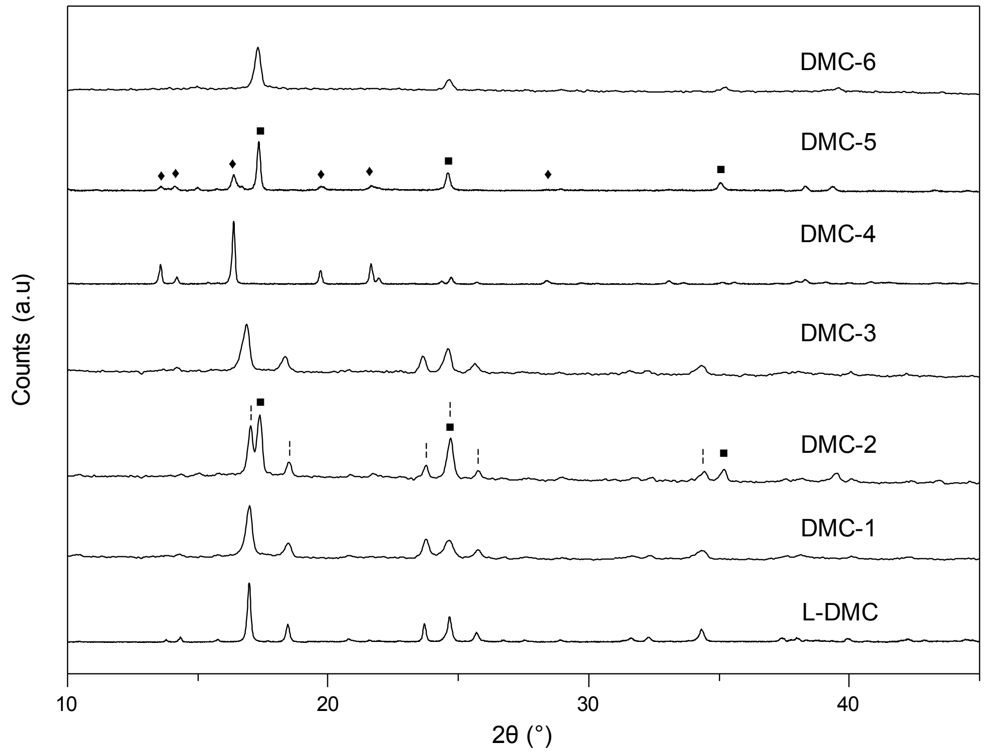

Fig. S1. XRD patterns of L-DMC and the different synthesized DMCs. Reflections corresponding to the cubic phase are denoted by (■), reflections corresponding to the layered phase are denoted by (¦) and reflections corresponding to the rhombohedral phase are denoted by (♦). The PXRD patterns of L-DMC, DMC-4 and DMC-5 were recorded on a Malvern PANalytical Empyrean diffractometer ($CuK_{\alpha1,2}$ radiation). The other PXRD data were collected on a STOE Stadi MP diffractometer ($CuK_{\alpha1}$ radiation).

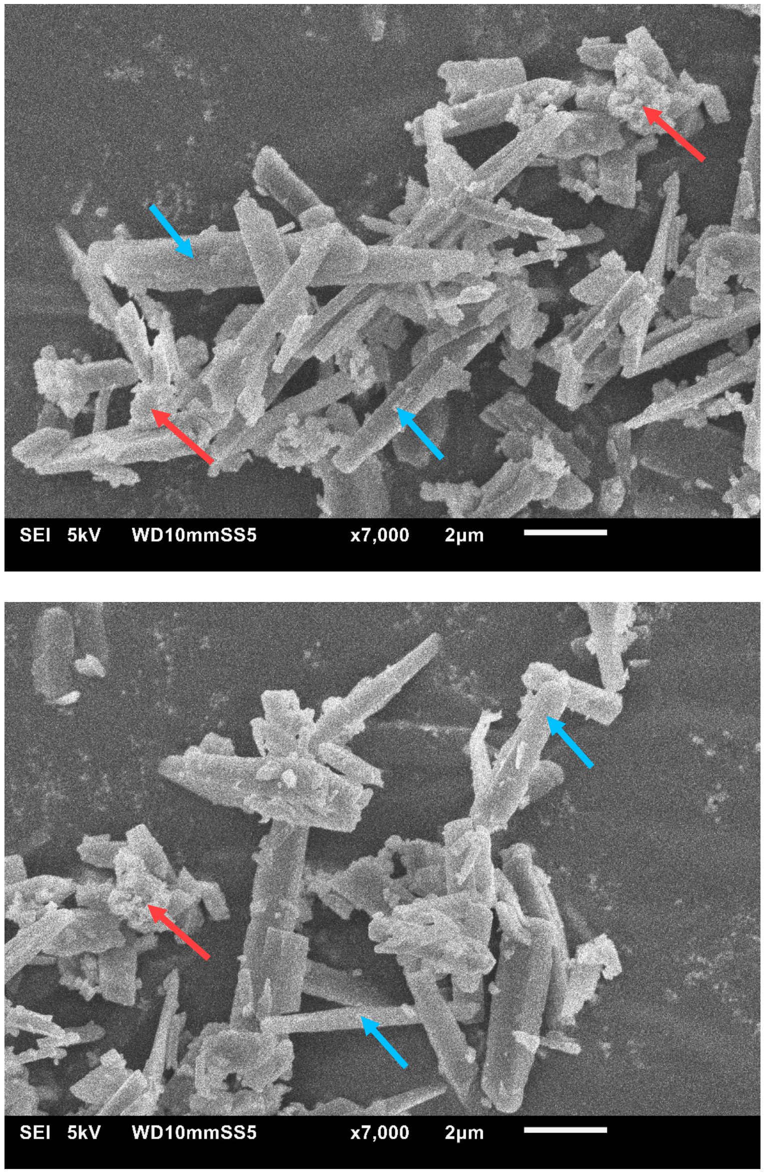

Fig. S2. SEM images of DMC-1. Two phases with different morphologies are discerned. Red arrows indicate the cubic phase and blue arrows indicate the layered phase.

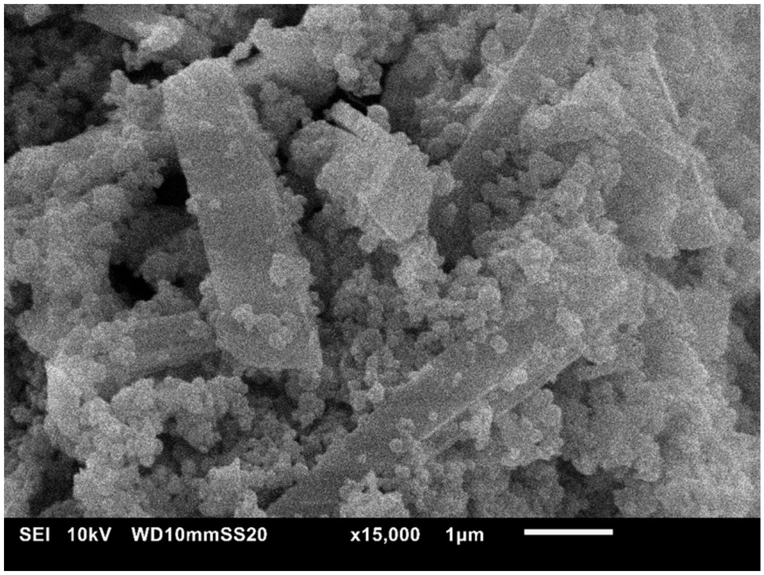

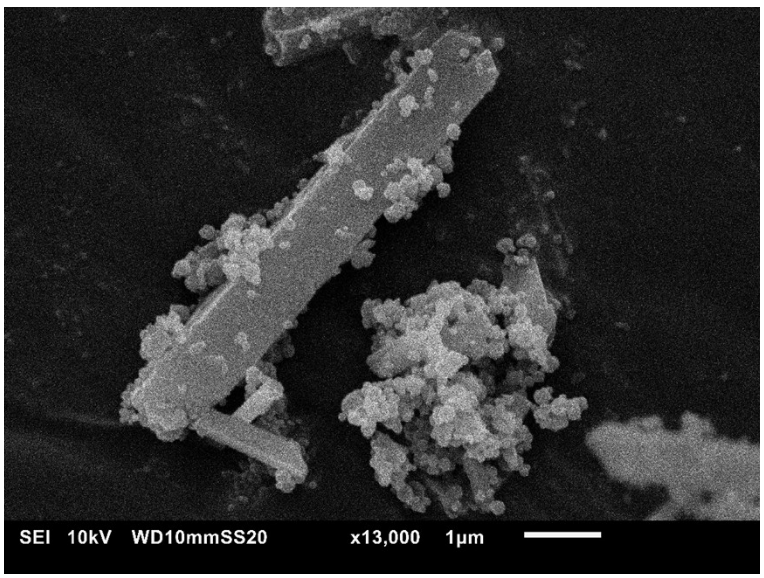

Fig. S3. SEM images of DMC-2. Two phases with different morphologies are clearly discerned.

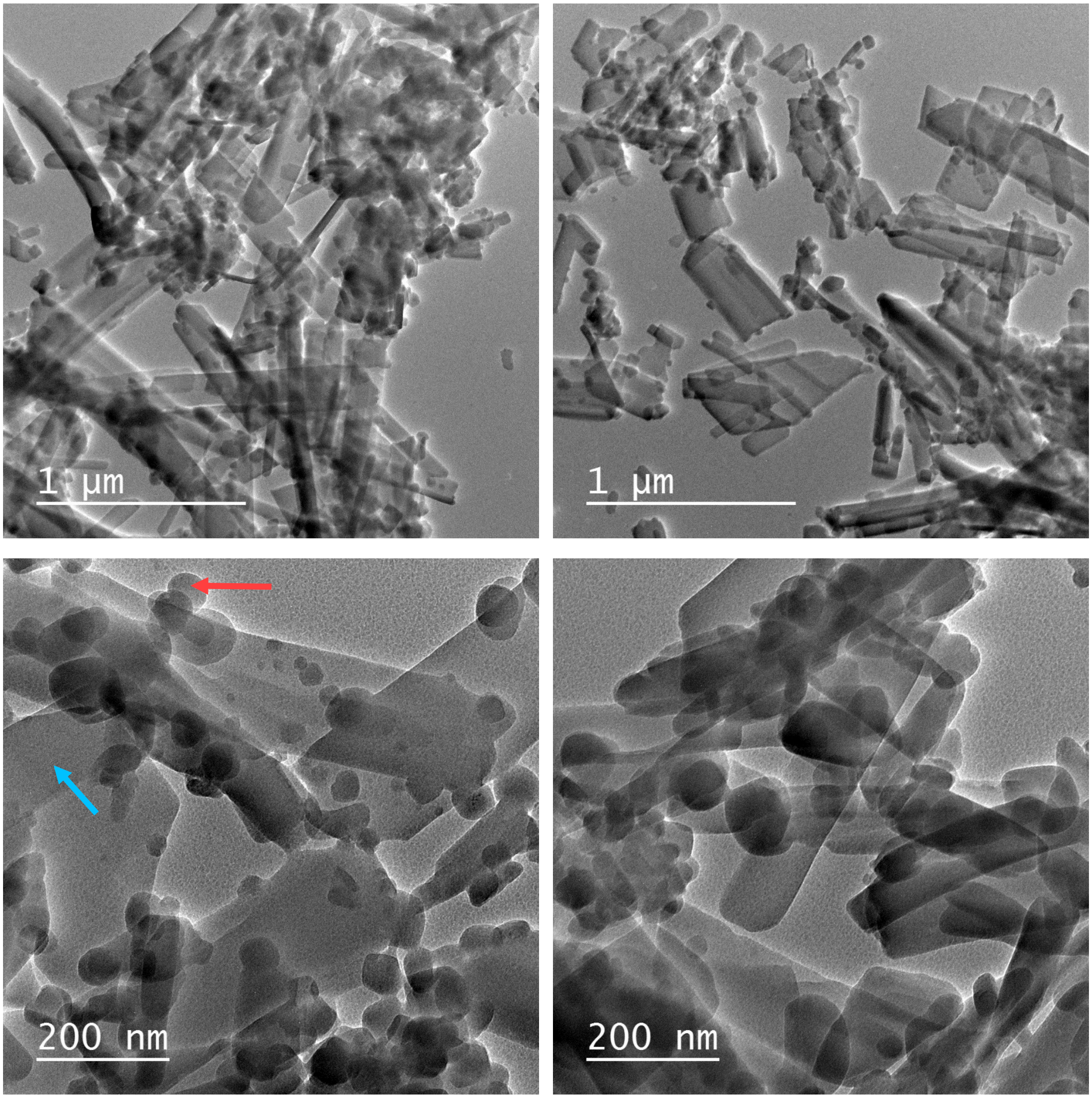

Fig. S4. TEM images of DMC-3. Two phases with different morphologies are clearly discerned. EDX analyses of the area signalized by a red arrow gave a Zn:Co molar ratio of 1.8 (close to the theoretical composition of the phase $Zn_3[Co(CN)_6]_2$). EDX analyses of the area signalized by a blue arrow gave a Zn:Co molar ratio of 2.0 (coinciding with the theoretical composition of the layered phase).

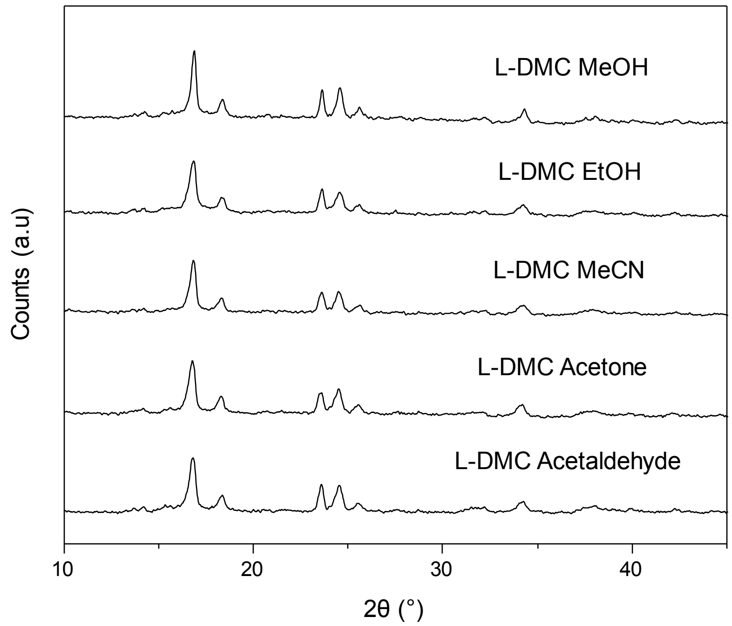

Fig. S5. XRD patterns of L-DMC after the AMOS dispersion procedure collected on a STOE Stadi MP diffractometer ($CuK_{\alpha 1}$ radiation).

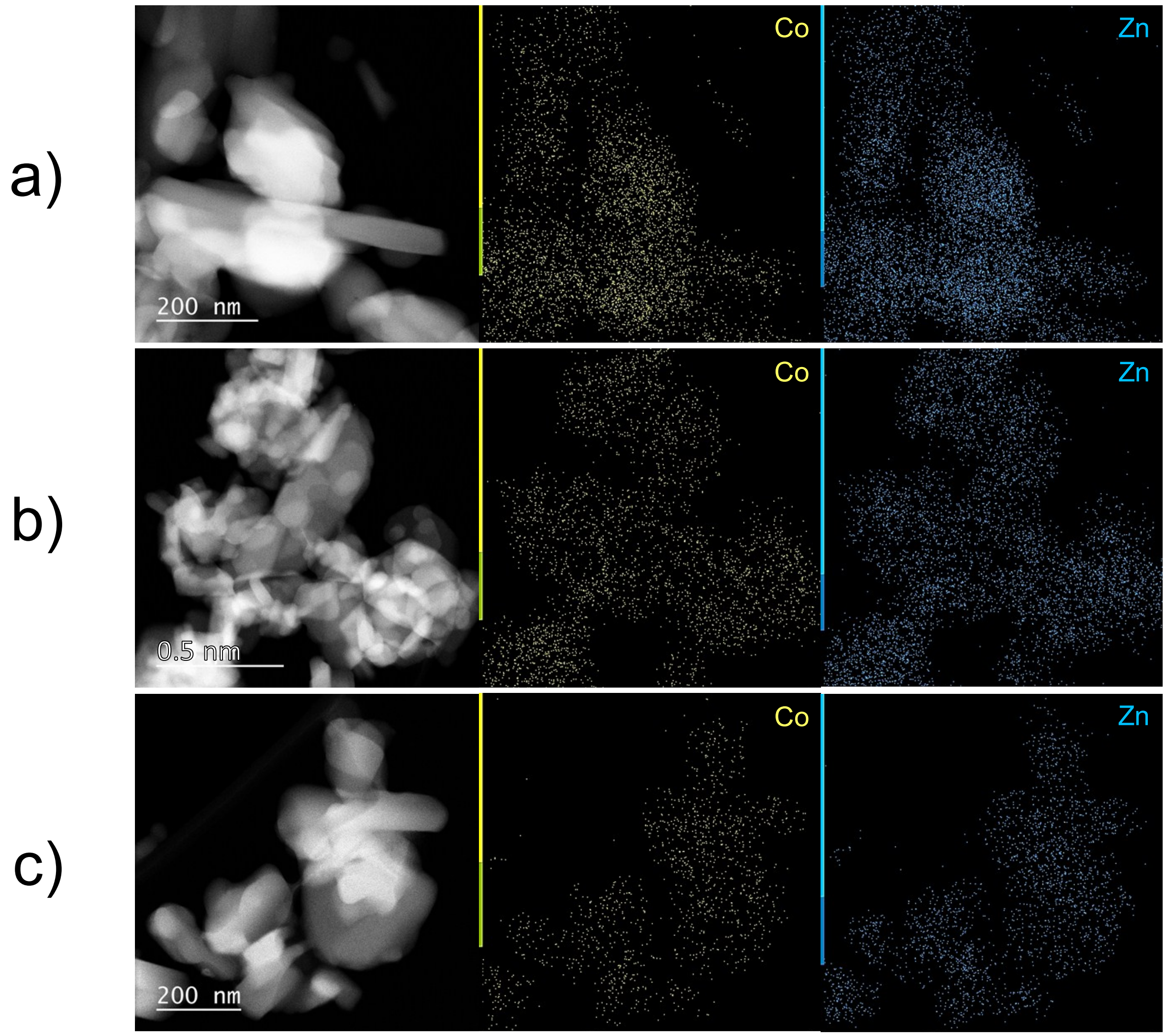

Fig. S6. HAADF-STEM images and EDX composition map for Co and Zn of three different areas (a, b and c) of L-DMC. EDX analyses of each area gave a Zn:Co molar ratio of 2.0 (coinciding with the theoretical composition of the layered phase).

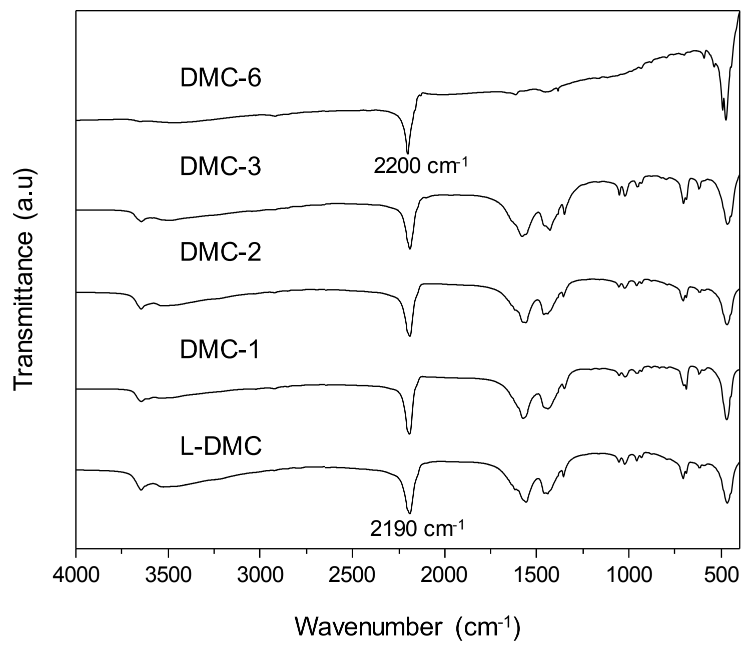

Fig. S7. FTIR spectra of selected samples.

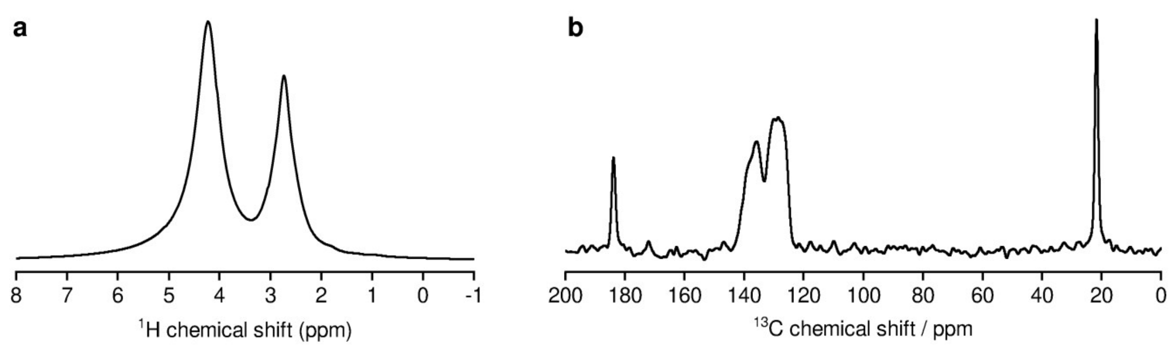

Fig. S8. ^{1}H MAS (a) and ^{13}C MAS (b) NMR spectra of L-DMC. The latter spectrum was recorded using Hahn-echo sequence with 90° and 180° pulses of 2.0 µs and 4.0 µs, respectively, and inter-pulse delay of 25 µs. Repetition delay between consecutive scans was 120 s and the number of accumulated scans was 1870. During the acquisition of the signal, high-power heteronuclear decoupling was applied. Integrated intensities of the ^{13}C MAS NMR signals better reflect the cyanide:acetate ratio than the intensities of the ^{1}H-^{13}C CPMAS NMR signals. We compared the intensities of the $-CH_3$ signal of acetate and the total cyanide signal, and obtained the cyanide:acetate ratio of 4.1. The disagreement between this value and the theoretical composition of L-DMC (cyanide:acetate ratio of 6) is mainly due to the very slow spin-lattice relaxation of the cyanide ^{13}C magnetization. With the repetition delay of 120 s, ^{13}C magnetization of cyanides could not be completely recovered, and therefore the corresponding NMR signals were partly suppressed.

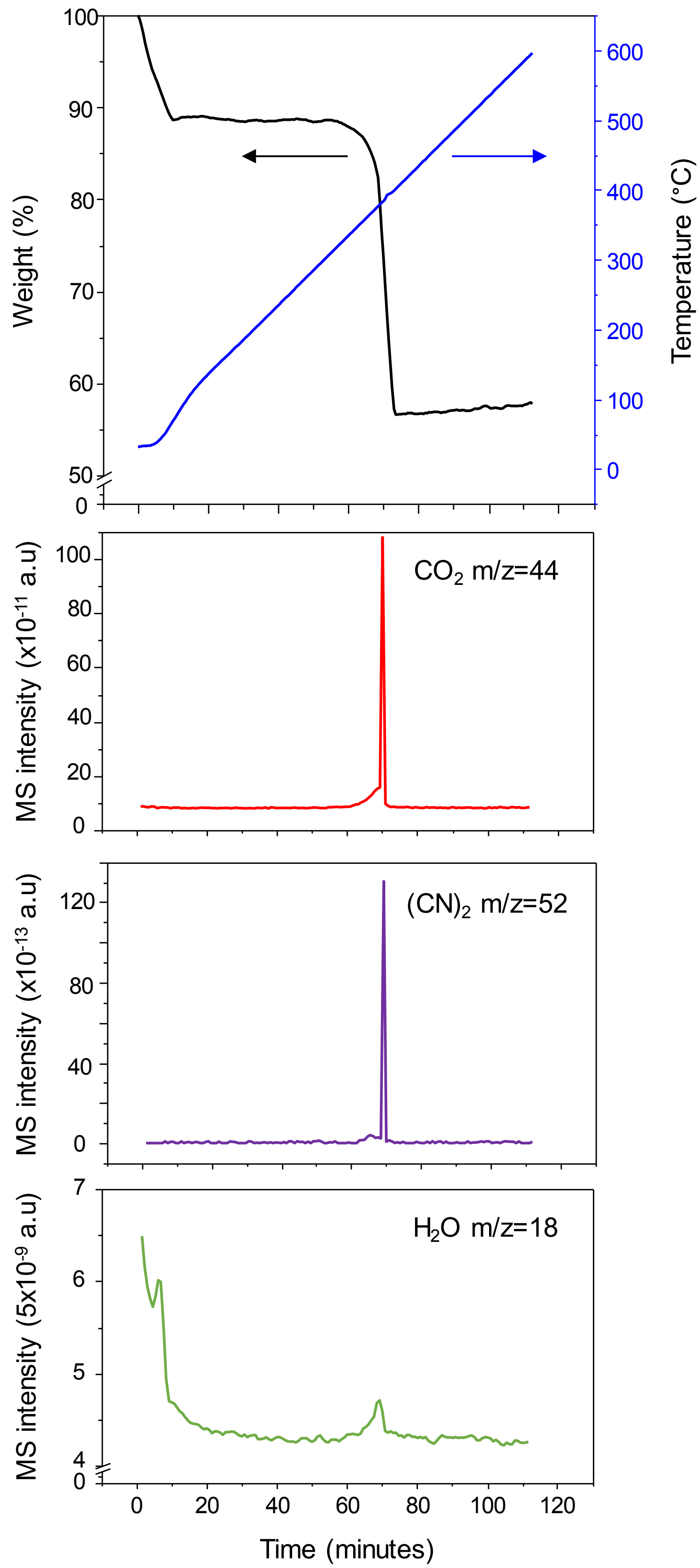

Fig S9. TG-MS analysis for L-DMC.

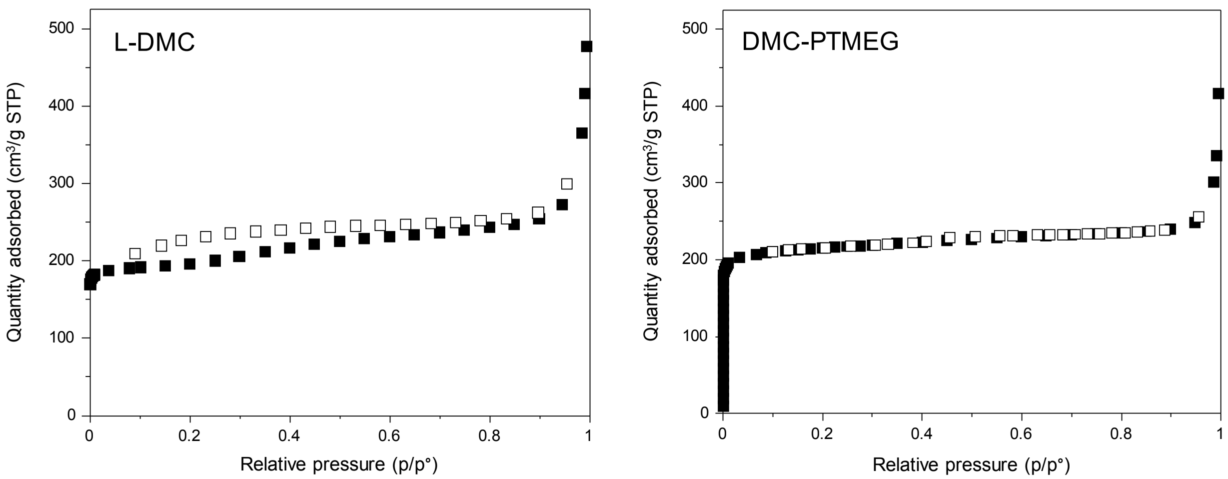

Fig. S10. Nitrogen physisorption isotherms of L-DMC and DMC-PTMEG (-196°C). Filled symbols denote adsorption and open symbols denote desorption.

Table S1. Textural properties determined from N_2 physisorption at -196°C of the L-DMC and DMC-PTMEG.

Sample	S_{BET} (m^2/g)	S_{ext} (m^2/g)
DMC-PTMEG	652	112
L-DMC	784	123

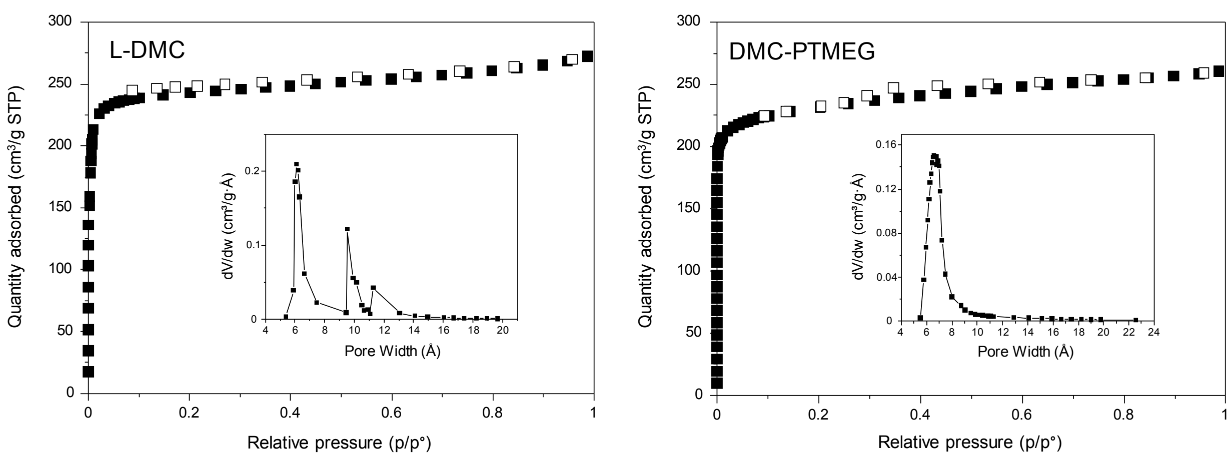

Fig. S11. Argon physisorption isotherms of L-DMC and DMC-PTMEG (-196°C). Filled symbols denote adsorption and open symbols denote desorption. Inset: Micropore size distribution estimated by the Horvath−Kawazoe method.

Table S2. Conversion of phenylacetylene and yield of the hydroamination product for selected DMC samples.

	4 h		24 h	
Catalyst	X (%)[a]	Y (%)[b,c]	X (%)[a]	Y (%)[b,c]
L-DMC	70	62	>99	87
DMC-1	10	9	31	25
DMC-3	55	45	97	80
DMC-4	2	2	10	10
DMC-5	35	26	81	65
DMC-6	43	36	80	65

[a] Conversion of phenylacetylene. [b] Yield of the hydroamination product based on phenylacetylene. [c] Acetophenone was the only side-product detected. Reaction conditions: phenylacetylene (0.5 mmol), 4-isopropylaniline (1 mmol), toluene (1 ml) as solvent and tetradecane (1 mmol) as internal standard, 50 mol% Zn, 110°C.

Table S3. Comparison of L-DMC with other Lewis acid catalysts.

Catalysts	X (%)[a]	Y (%)[b,c]	r_0 (mmol/h)[d]
L-DMC	>99	87	0.87
DMC-PTMEG	98	82	0.06
Zn/BEA[e]	75	40	0.04
[Zn-Al] LDH[f]	16	12	<0.01
[Zn-Al] MMO[f]	13	11	<0.01
ZnO[g]	6	4	<0.01

[a] Conversion of phenylacetylene after 24 h reaction time. [b] Yield of the hydroamination product based on phenylacetylene after 24 h reaction time. [c] Acetophenone was the only side-product detected. [d] Initial reaction rate of hydroamination reaction expressed as mmol of imine produced per h. [e] The solid was prepared by impregnation of a commercial Beta zeolite (CP811BL25, Si/Al = 12.5) with $ZnCl_2$ (Zn wt.% = 11%). [f] The solids were synthesized following literature procedures [1,2]. [Zn-Al] layered double hydroxide, Zn wt.% = 35% and [Zn-Al] mixed metal oxide, Zn wt.% = 53%. [g] ZnO nanoparticles 40-100 nm (Alfa Aesar), Zn wt.% = 80%. Reaction conditions: phenylacetylene (0.5 mmol), 4-isopropylaniline (1 mmol), toluene (1 ml) as solvent and tetradecane (1 mmol) as internal standard, 50 mol% Zn, 110°C.

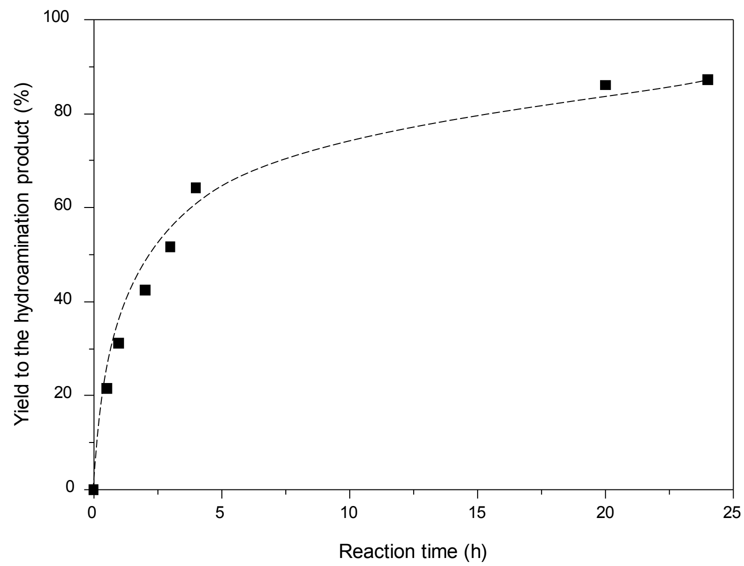

Fig. S12. Yield to hydroamination product vs. time plot. Reaction conditions: phenylacetylene (0.5 mmol), 4-isopropylaniline (1 mmol), toluene (1 ml) as solvent and tetradecane (1 mmol) as internal standard, 50 mol% Zn, 110°C.

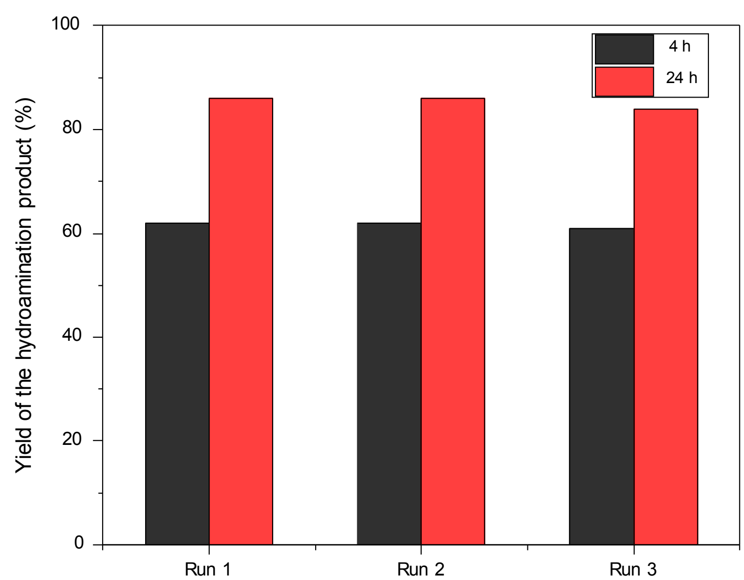

Fig. S13. L-DMC Recycling test. Full phenylacetylene conversion was achieved in each run after 24 h reaction time. Reaction conditions: phenylacetylene (0.5 mmol), 4-isopropylaniline (1 mmol), toluene (1 ml) as solvent and tetradecane (1 mmol) as internal standard, 50 mol% Zn, 110°C.

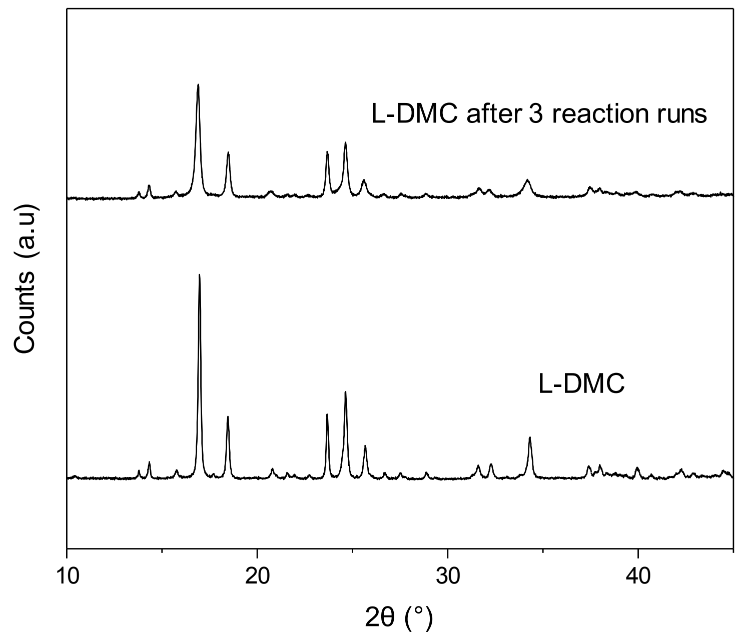

Fig. S14. XRD pattern of L-DMC before and after 3 reaction runs. Reaction conditions: phenylacetylene (0.5 mmol), 4-isopropylaniline (1 mmol), toluene (1 ml) as solvent and tetradecane (1 mmol) as internal standard, 50 mol% Zn, 110°C, 24 h.

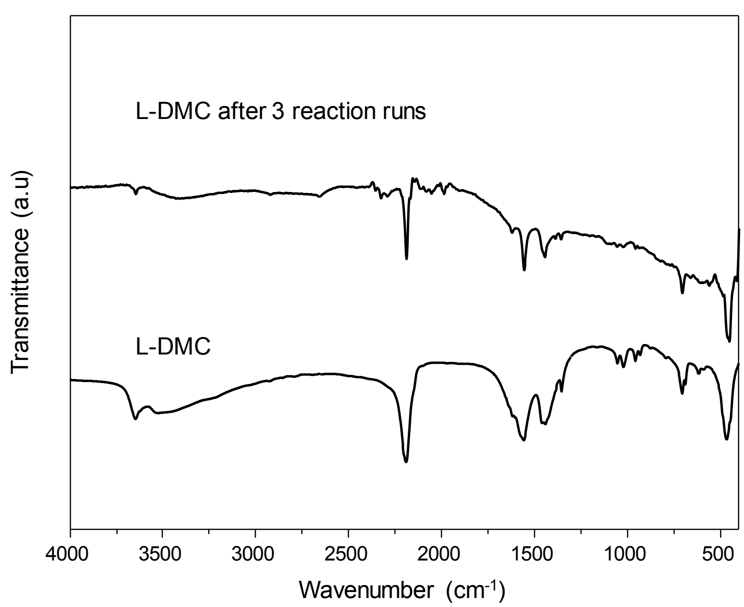

Fig. S15. FTIR spectra of L-DMC before and after 3 reaction runs. Reaction conditions: phenylacetylene (0.5 mmol), 4-isopropylaniline (1 mmol), toluene (1 ml) as solvent and tetradecane (1 mmol) as internal standard, 50 mol% Zn, 110°C, 24 h.

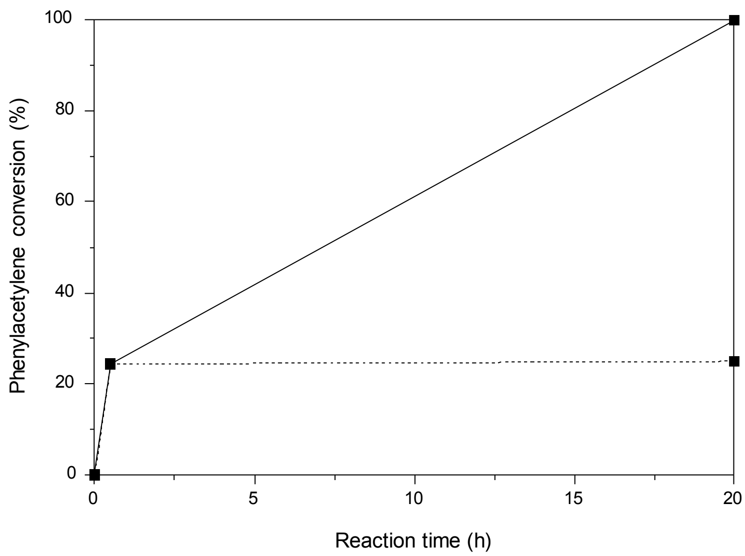

Fig. S16. L-DMC hot filtration test. Dashed line represents the conversion after removal of the catalyst. Reaction conditions: phenylacetylene (0.5 mmol), 4-isopropylaniline (1 mmol), toluene (1 ml) as solvent and tetradecane (1 mmol) as internal standard, 50 mol% Zn, 110°C.

References

1. K. Abderrazek, F. Srasra Najoua, E. Srasra, *Appl. Clay Sci.*, 2016, **119**, 229–235.

2. T-T. H. Nguyen, X-T. Thi Nguyen, C. Q. Nguyen, P. H. Tran, *Heliyon*, 2018, **4**, e00966.